Hindawi
Advances in Materials Science and Engineering
Volume 2019, Article ID 8979864, 12 pages
https://doi.org/10.1155/2019/8979864

Research Article

Influence of Hydrophobic Coating on Freeze-Thaw Cycle Resistance of Cement Mortar

Zijian Song[1,2] **Zhongyuan Lu**[1] **and Zhenyu Lai**[1]

[1]*School of Materials Science and Engineering, State Key Laboratory for Environment-Friendly Energy Materials, Southwest University of Science and Technology, Mianyang 621010, China*
[2]*Mianyang Vocational and Technical College, Mianyang 621000, China*

Correspondence should be addressed to Zijian Song; szj2009189@163.com and Zhongyuan Lu; luy@swust.edu.cn

Received 25 June 2019; Revised 8 August 2019; Accepted 10 October 2019; Published 6 November 2019

Guest Editor: Carlos Alves

Due to the porous characteristics of cement-based materials, they are often corroded by salt solutions, which results in decreased durability, especially against damage under freeze-thaw cycles (FTCs). Improving surface properties is an effective way to improve the durability of these materials. In this study, a hydrophobic coating was applied to the surface of cement mortar by chemical modification of low surface energy materials. Fourier transform infrared spectroscopy (FT-IR) showed that low surface energy substances are linked to hydration products through chemical bonds. A water contact angle test indicates that the surface of cement mortar changed from hydrophilic ($\theta = 14^{\circ}$) to hydrophobic ($\theta = 140^{\circ}$) after chemical modification. The cumulative water uptake of hydrophobic samples decreased by 90%. Meanwhile, the wear resistance of the hydrophobic coatings was excellent. Compared with the baseline sample, mass loss rate, flexural strength, and compressive strength of hydrophobic coating samples increased several-fold in the FTC test. Microstructural changes of the mortar were characterized by scanning electron microscopy. The results show that a hydrophobic coating can significantly improve the freeze-thaw resistance of cement-based materials. The formation of a hydrophobic layer on the surface of cement-based materials can improve their durability. The research results not only have applications in civil engineering but will also have great impact in the restoration of historic structures.

1. Introduction

Concrete is a type of building material based on cement with highly effective mechanical properties; it is widely used as a structural material for buildings, bridges, undersea tunnels, etc. In ancient times, cementitious materials made from calcium hydroxide and clay were often used to build what have become today's world-famous historical buildings, such as the Pantheon in Rome. However, both modern and historical buildings are usually corroded by salt solutions, by which water penetrates the concrete, which is a factor contributing to concrete degradation. The freeze-thaw cycle (FTC) in severely frozen regions will cause sustained damage to concrete due to osmotic pressure, water expulsion, and in-pore crystallization during the FTC process [1–6]. Researchers have proposed many methods to improve the FTC resistance of cement-based materials, such as adding air-entraining substances [7–10], pozzolanic minerals, or fiber admixtures [11–24]. The first method can relieve crystallization pressure in the FTC, while the latter method can improve the compactness of the concrete. However, the aforementioned methods lead to negative impacts on the concrete, such as deteriorating mechanical properties, difficult workability, and increased drying shrinkage.

Super-hydrophobic phenomena exist widely in nature [25–32]. Previous studies have pointed out that two basic requirements must be met for the surface of a solid material to be super-hydrophobic: (1) microscale and nanoscale rough structures and (2) lower surface free energy. Researchers have accurately expressed this theory through the Wenzel model [33] and Cassie–Baxter model [34].

Based on the above research, super-hydrophobic coatings have been applied to concrete surfaces for waterproofing, deicing, and self-cleaning [35–40]. Super-

hydrophobic coatings can be prepared by bonding low surface energy materials to the concrete surface. Materials such as polytetrafluoroethylene (PTFE), polyether ether ketone (PEEK), and silanized diatomaceous earth (DE) are bonded to the concrete surface by epoxy resin to obtain a super-hydrophobic surface [41]. Besides, super-hydrophobic surfaces can also be obtained by bonding super-hydrophobic rice husk ash [42], paper sludge ash [43], or nanosilica gel [34] to the concrete surface. Another way to obtain super-hydrophobic surfaces is the template method, where the features of micropillared molds made of poly-dimethylsiloxane (PDMS) are replicated immediately after demolding, and then siloxane-based compounds are sprayed to form a low energy surface [44].

Due to the excellent waterproofing effect of super-hydrophobic coatings, the water absorption of concrete decreases significantly, but the durability of such coatings is insufficient and they can easily fall off. Up to now [37], there has been a lack of research on the mechanical stability of super-hydrophobic coatings; therefore, the application of super-hydrophobic coatings in engineering is limited. To solve this problem, a vacuum impregnation process was adopted in this study. Such technology is more suitable for performance improvement of prefabricated concrete structures, similar to the anticorrosion treatment of steel structures. Through this technology, low surface energy materials (iso-octyltriethoxysilane) can penetrate the cement mortar and combine with the cement hydration products, such as calcium hydroxide and ettringite, to form a continuous self-assembled molecular film layer. This molecular film layer reduces the surface energy of the mortar, thus achieving chemical modification of the rough surface of the mortar to form a hydrophobic coating. The wetting property was characterized by a water contact angle (WCA) test. A water absorption test and FTC resistance test were used to evaluate the protective effect of the hydrophobic coating on mortar blocks. Building structures are often subjected to external forces, which may result in surface wear and tear. Thus, the wear resistance was tested by sandpaper polishing under a certain pressure, after which the change of water absorption was tested. The microstructure of the cement mortar was characterized by scanning electron microscopy (SEM). Interface chemical reactions were characterized by Fourier transform infrared spectroscopy (FT-IR).

2. Materials and Methods

2.1. Materials. Ordinary Portland cement (OPC) was used as the binding material in all mortar specimens. The chemical composition of the OPC is shown in Table 1. The aggregates were acquired from Xiamen ISO Standard Sand Co., Ltd., with particle diameters ranging from 0.5 to 2.0 mm. Iso-octyltriethoxysilane was acquired from Wacker Chemicals. Tap water was used in the preparation of mortar samples. Anhydrous ethanol was acquired from Cormio Inc, China. To ensure permeability, iso-octyltriethoxysilane was used as a low surface energy material for surface treatment with a concentration of 2%, with the remainder composed of ethanol (28%) and water (70%).

2.2. Preparation. The proportions used to prepare the mortar samples and their properties after 28 days of curing are shown in Table 2. To ensure the uniformity of all mortar blocks, the following mixing process was adopted: (1) 450 g of cement and 225 g of water were added to the mixer and stirred for 60 s at slow speed; (2) 1350 g of sand was added evenly for 30 s; (3) the mixture was stirred at high speed for 30 s; (4) the mixer was stopped for 90 s for manual mixing; and (5) the mixture was further stirred for 60 s at high speed. After the concrete mixture was mixed, it was horizontally poured into a cuboid mold (40 mm × 40 mm × 160 mm) and a cubic mold (40 mm × 40 mm × 40 mm). After molding, all specimens were wet cured for 24 h (RH = 100% and $T = 21 \pm 1^{\circ}C$) and then demolded and cured for 28 days in water ($21 \pm 1^{\circ}C$). The cuboid specimen was used for the FTC test, and the cubic specimen was used for water absorption and wear resistance tests.

To ensure the effective penetration of modifiers, the hydrophobic coating on the surface of the mortar specimen was prepared using an osmosis vacuum degassing device (Figure 1). After curing for 28 days, the sample was dried to a constant weight and placed in the vacuum tank. When the vacuum was below 20 kPa, the iso-octyltriethoxysilane solution was slowly infused into the vacuum tank until it inundated the entire sample. Then, the hydrophobic coating was applied to the mortar surface after drying at 60°C for 12 h.

2.3. Test Methods. The WCA was measured using a contact angle tester (KRUSS, K100, Germany). It was determined using deionized water (2.5 μL deposited with a micropipette) and by calculating the average of three measured values on the surface.

The capillary water absorption test was used to quantify the ability of the concrete to absorb water by capillary suction. To evaluate the hydrophobicity, the baseline samples and hydrophobic samples were placed in water under atmospheric pressure (101 kPa) and vacuum (20 kPa) for two days each. The weights of the samples were recorded before and after immersion to calculate the mass uptake of water. An MPD-2 metallographic polisher (Shanghai Zhongyan Instrument Co., Ltd., China) was used to determine the wear resistance of the mortar. As the polisher rotates, the sandpaper begins to slide and creates friction with the surface of the sample under pressure, such that the microstructure of the sample surface will be destroyed. After polishing, the mass loss rate was calculated and the mass uptake of water was measured. 240-grit sandpaper was fixed on the turntable of the polisher, and the turntable rotated at 500 rpm. The longer the polishing time, the higher the wear degree of the test block. In this study, the lengths of polished mortar blocks indicate the degree of wear.

The KDR-A rapid freeze-thaw circulator (Beijing Kangluda Test Instrument Co., Ltd., China) was used to determine the FTC resistance (Figure 2). The sample was immersed in water for two days and then put into the rubber sleeve of the circulator, which was filled with water. The temperature cycle consisted of freezing and heating stages

Table 1: Chemical composition of ordinary Portland cement (P. O42.5R).

	Chemical composition (%)									
	SiO_2	Al_2O_3	CaO	Fe_2O_3	MgO	K_2O	TiO_2	Na_2O	SO_3	Others
Cement	19.26	4.33	65.46	3.06	1.60	0.77	—	0.13	4.45	0.94

Table 2: Mix proportions and mechanical properties of the mortar.

Water-cement ratio	Raw material (g)			Density (kg/m^3)	Mechanical parameter at 28 d (MPa)	
	Cement	Water	Sand		Compressive strength	Flexural strength
0.5	450	225	1350	2300	52.4	12.8

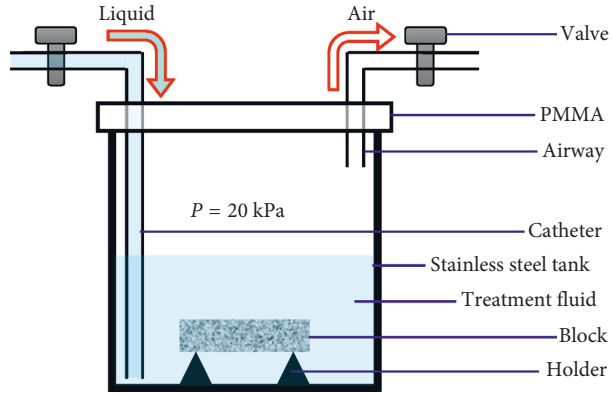

Figure 1: Schematic of osmosis vacuum degassing device.

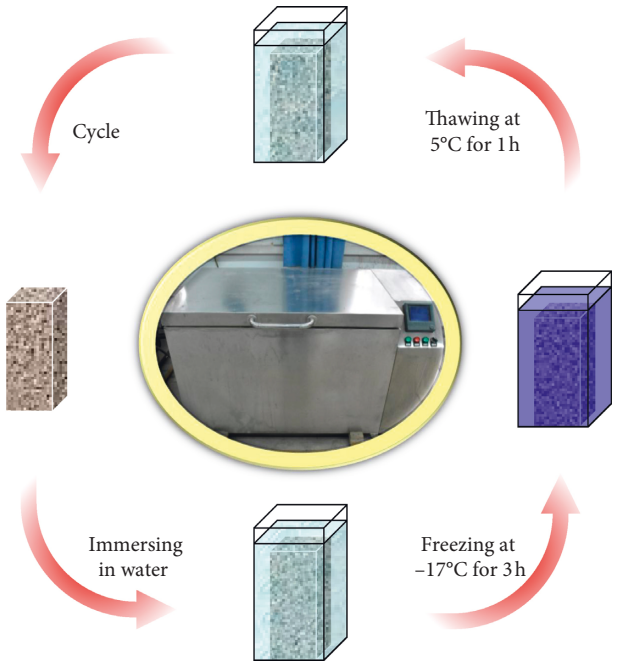

Figure 2: Schematic of the freeze-thaw cycle (FTC) test.

and took approximately four hours in total. During the freezing stage, the water temperature dropped from 5°C to −17°C after 2.5 h. During the melting stage, the water temperature rose from −17°C to 5°C after 1.5 h. With an increase in the FTCs, the damage degree of the samples increased. After FTC damage, the mass loss rates and flexural and compressive strengths of the samples were measured to evaluate their degrees of damage.

The microscopic morphologies of the samples were observed by SEM (MAIA3, TESCAN, Czech Republic). Fourier transform infrared spectroscopy (FT-IR) spectra were acquired in the range of 400–4000 cm^{-1} with an IR spectrophotometer (380FTIR, Thermo Fisher Scientific, America). The flexural and compressive strengths of the mortar were evaluated on the same testing machine (SANS CMT5105, Shenzhen, China) at a loading rate of 2400 ± 200 N/s.

3. Results and Discussion

3.1. Wetting Properties and Water Contact Angle. Without changing the surface microstructures of the mortar specimens, the surface of the mortar shows good hydrophobicity only through iso-octyltriethoxysilane solution modification, as shown in Figure 3(b). This phenomenon can be explained by the Wenzel theory that a hydrophobic surface can be obtained by modifying the rough mortar sample with low surface energy materials. First, iso-octyltriethoxysilane is hydrated to produce silanols (Si-OH). Secondly, silanol is combined with quartz sand, hydrated C-S-H gel, ettringite, and calcium hydroxide through -OH group reactions. Finally, the two -OH groups of iso-octyltriethoxysilane form Si-O-Si bonds by condensation while

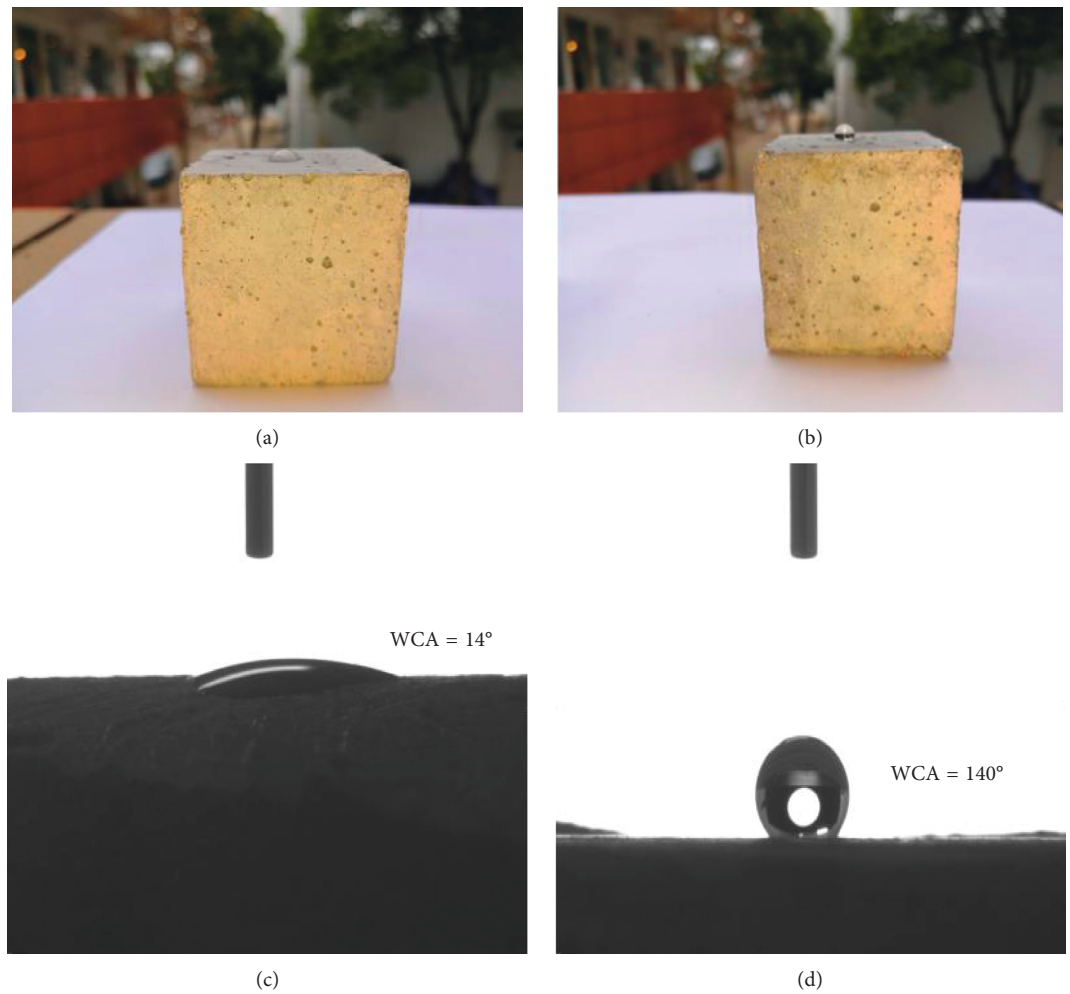

Figure 3: Water contact angles on the surface of mortar specimens: (a) baseline sample, (b) hydrophobic sample, (c) WCA of the baseline sample, and (d) WCA of the hydrophobic sample.

releasing water. After the above reaction, iso-octyltriethoxysilane forms a continuous self-assembled molecular film on the surface of the hydrated products. Iso-octyltriethoxysilane contains a $-CH_3$ group and $-CH_2$ group which effectively reduce the surface energy of the cement mortar. Therefore, the rough surface structure modified by low surface energy materials exhibits excellent hydrophobic properties.

Figure 3(c) shows that the contact angle of the baseline sample is approximately 14°, indicating that the porous, rough surface of the mortar belongs to the hydrophilic surface. Figure 3(d) shows that the WCA of the modified mortar surface increases to 140°, which proves that a hydrophobic surface can be obtained by modifying the rough hydrophilic surface with low surface energy materials. The WCA of the modified mortar surface did not reach a super-hydrophobic state ($\theta > 150$) because the surface roughness of the mortar itself did not conform to the Cassie–Baxter model. The fragile micro/nanostructure is not conducive to the wear resistance of the coating itself. Therefore, the obtained WCA ($\theta = 140°$) is sufficient to improve the waterproof performance of the mortar.

3.2. Water Absorption. The influence of the hydrophobic coating on the water absorption of the mortar samples is shown in Figure 4. The results show that the cumulative water uptake of the baseline sample increased gradually from the beginning to achieve equilibrium and remained at a stable level thereafter, while the water absorption of the hydrophobic sample remained at a low level. After 15 days of immersion, the cumulative water uptake of the hydrophobic samples was reduced by 90%. This excellent waterproofing effect is equivalent to the waterproofing effect of a nanocomposite waterproof coating [45].

The microscale rough structure of the mortar surface is modified by the low surface energy material to reach a Wenzel state, which shows an excellent waterproofing effect. The unmodified samples retain the hydrophilic properties of the cement-based materials.

3.3. Wear Resistance and Thickness of the Hydrophobic Coating. Fragile micro/nanostructures on hydrophobic surfaces are susceptible to damage, leading to degradation of the hydrophobic properties. In this research, to test the wear resistance of the hydrophobic coating, the mortar sample

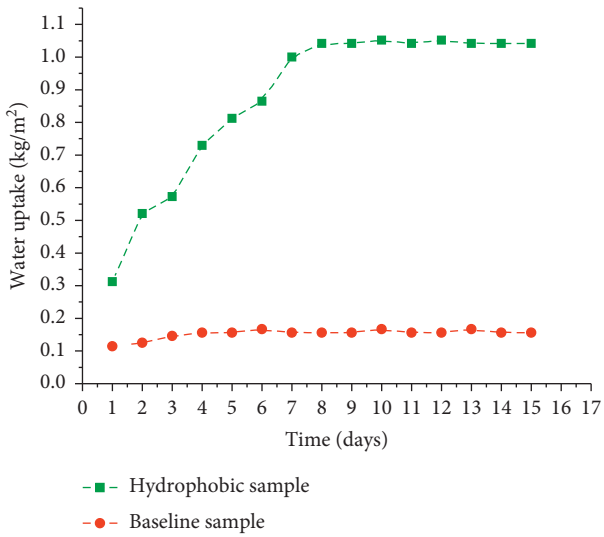

FIGURE 4: Water absorption results for the baseline and hydrophobic samples.

was placed on a burnisher and polished with 240-grit sandpaper at 500 rpm, and then the water absorption was tested. The lengths of the mortar blocks after polishing indicate their degrees of wear. Table 3 lists the length reductions corresponding to different polishing times.

As shown in Figure 5(c), after polishing, the WCA ($\theta = 77^{\circ}$) of sample 5 decreased but remained between that of the baseline sample as shown in Figure 5(a) and that of the unpolished hydrophobic sample as shown in Figure 5(b). Because the thickness of the chemically modified mortar reaches the range of 1–3 mm, the hydrophobic sample remains hydrophobic even after the rough surface structure is destroyed. In the next section, the mass loss and water absorption after polishing are discussed. Figure 6(f) shows that the mass loss rate of the samples increases with an increase in length reduction. The mass loss rate of the sample is the largest, and its WCA ($\theta = 77^{\circ}$) is still significant. Samples 1, 3, and 5 were immersed in water for 15 days with the baseline sample (Figure 6(a)) and the unpolished hydrophobic sample (Figure 6(b)). When the samples were immersed in water, many bubbles were observed on the surface of the baseline sample (Figure 6(a)). In contrast, we could see only a few bubbles on the surface of the hydrophobic sample (Figure 6(b)), even if it was reduced by over 10 mm by the sandpaper (Figure 6(e)). Surface bubbles are formed when water enters the sample and displaces air from the sample. A few bubbles on the surfaces of the polished samples show that the hydrophobic coating maintains an excellent waterproofing performance even after polishing. In the cumulative water uptake test, it was also proved that the hydrophobic coatings have excellent wear resistance, as shown in Figure 7.

In Figure 7, the water absorption curve shows that the cumulative water uptake of the polished hydrophobic samples remained at a low level. This phenomenon shows that the wear resistance of the hydrophobic coating is outstanding. The surface of the hydrophobic coating is worn after polishing, which leads to decreased WCA, but it still maintains excellent waterproof properties. This phenomenon can be explained by Figure 8.

Figure 8 illustrates the thickness of the hydrophobic coating by wetting the cross section with water. In this figure, the light hydrophobic coating can be observed continuously around the perimeter of the dark central area, which indicates that a continuous hydrophobic coating was formed on the surface of the sample by vacuum impregnation. The thickness of the hydrophobic coating is within the range of 1–3 mm. This is a reasonable explanation for the hydrophobic properties of the polished hydrophobic samples decreasing after polishing but the waterproof properties remaining excellent. When iso-octyltriethoxysilane penetrates the mortar sample, self-assembled membranes will form on the surface of the hydrated particles. As the interior of the mortar is rough and porous, a stable hydrophobic network structure with a certain thickness is obtained. In this way, even if the surface of the microscale rough structure is destroyed, the network structure can still play a perfect waterproofing role.

3.4. FTC Resistance Analysis. As shown in Figure 9, steep curves for the mass loss rate and flexural and compressive strengths were observed for the baseline sample after the FTC tests. On the contrary, the corresponding curves for the hydrophobic samples change more smoothly. This phenomenon shows that the baseline sample was severely damaged after the FTCs, while the hydrophobic sample was much less damaged due to the protection of its hydrophobic coating. After 36 FTC tests, the mass loss rate of the baseline sample was approximately 48.0 wt.%. Meanwhile, the flexural and compressive strengths of the baseline sample were reduced to 0.3 MPa and 11.0 MPa, respectively. After 36 FTC tests, the mass loss rate and flexural and compressive strengths of the hydrophobic sample were 0.8 wt.%, 7.5 MPa, and 38.2 MPa, respectively. After 48 FTC tests, the baseline sample lost its original morphology and size (Figure 10) because its mass loss rate was over 62 wt.%. In contrast, the original morphology and size of the hydrophobic sample remained after 72 FTC tests (Figure 10). The test results show that the mass loss rate and flexural and compressive strengths of the hydrophobic sample are 10.4 wt.%, 1.0 MPa, and 16.5 MPa, respectively, which are very close to the values of the baseline sample after 24 FTCs. The test results indicate that the hydrophobic coating not only has an excellent waterproofing effect but it also has excellent anti-FTC performance. Due to the protective effect of the hydrophobic coating, water cannot impregnate the sample, thus alleviating damage from FTCs. Exfoliation of the surface coating of the hydrophobic sample occurred at the 36^{th} cycle. This is because the sample had been immersed in water at below 0°C. The sample was encapsulated by external ice, which produced certain stresses and destroyed the hydrophobic coating. It is predicted that increasing the hydrophobic coating thickness will effectively improve the FTC resistance of the samples. This will be further explored in future research. The improvement of frost resistance was also observed in concrete modified with metakaolin and

Table 3: Length reduction of the modified sample.

Sample number	Radius of turntable (mm)	Burnisher revolutions per minute	Polish time (min)	Polish distance (km)
1	100	500	0.5	0.3
2			4.5	2.8
3			8.5	5.4
4			12.5	7.9
5			16.6	10.4

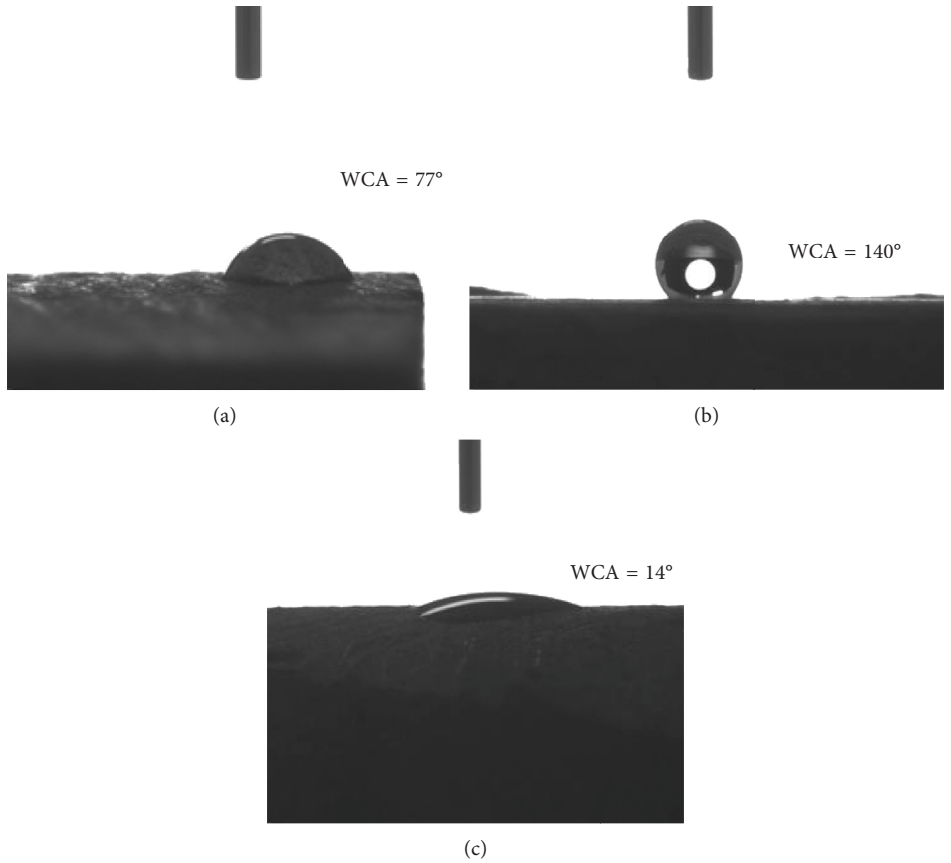

Figure 5: WCA of the (a) baseline sample, (b) hydrophobic sample, and (c) polished hydrophobic sample.

nanoparticles [46]. This is an entirely different technical concept from the hydrophobic coating, but it can be combined to achieve better frost resistance in future research.

3.5. Microscopic Analysis and Chemical Characterization. To study the effect of the FTC on the internal structure of the mortar, the sectional microstructures of the hydrophobic and the samples were compared after enduring FTC damage (Figure 11). As shown in Figure 11(a), after the 12^{th} FTC test, a visible crack could be seen on the baseline sample. Moreover, the crack was further extended due to the continuous damage from FTC after the 36^{th} FTC test. The width of the crack increased from 2.1 μm to 4.3 μm (Figure 12(b)). Significantly, only cracks less than 1 μm (Figure 11(c)) could be observed on the hydrophobic sample after the 12^{th} FTC test. After the 48^{th} FTC test, a crack becomes evident with a width of approximately 1 μm (Figure 11(d)). As exhibited in Figure 11(e), the width of the crack is still below 4 μm after the 72^{nd} FTC test. Figure 11(f) displays the microstructure of the hydrophobic coating on the mortar block after enduring 72 FTCs, indicating that the hydrophobic coating could effectively reduce the damage to the mortar caused by FTCs. Based on this, we can confidently predict that the FTC resistance of the mortar block would be improved by increasing the thickness of the hydrophobic coating.

As shown in Figure 12(a), the hydrophobic coating appeared after the sample section was wet with water. In Figure 12(b), by magnifying by 20,000 times, the SEM images show that the interior of the mortar is filled with acicular or flaky hydration products. This micron-scale rough structure is one of the conditions for the formation of the hydrophobic coating. The chemical modification of the

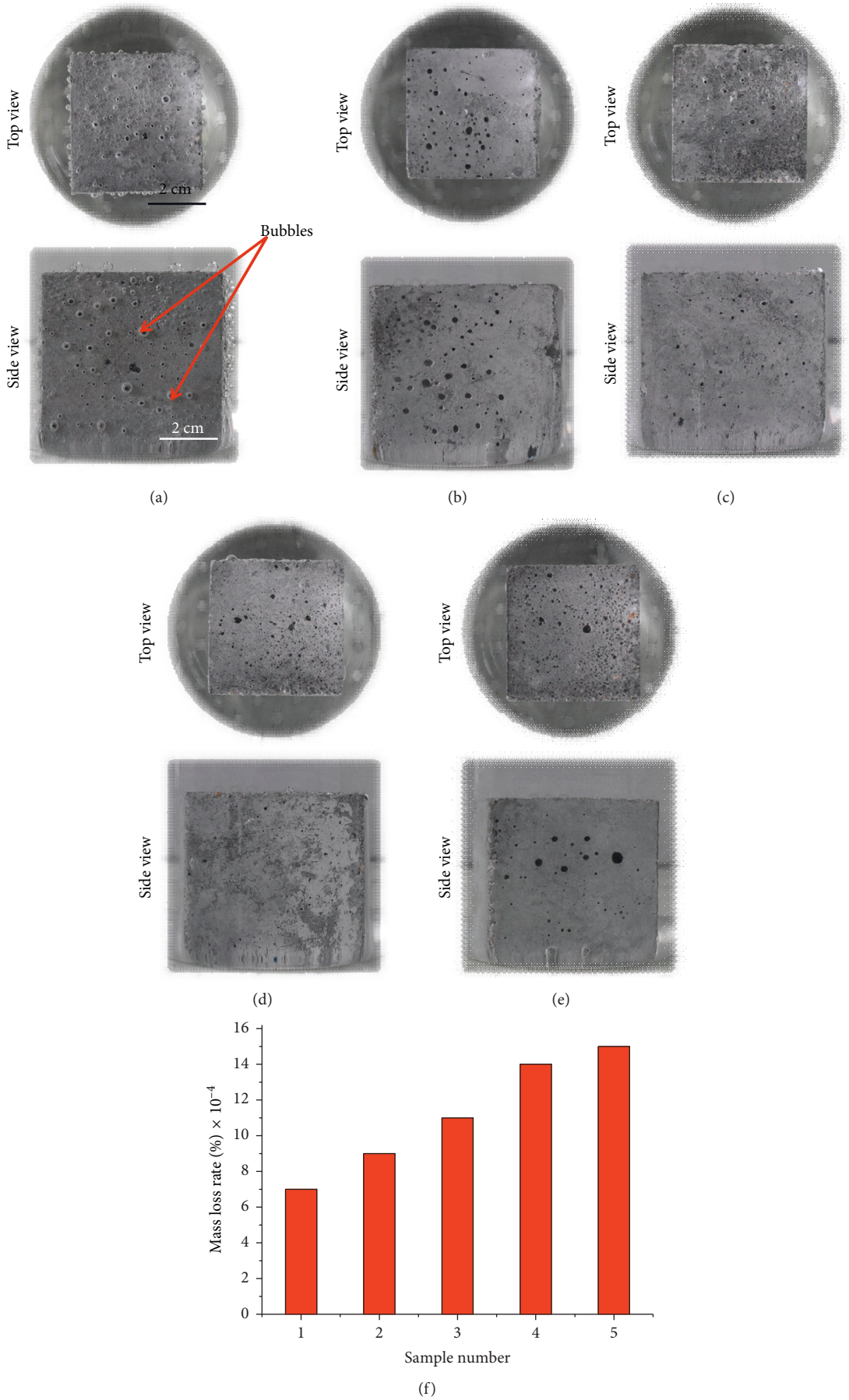

Figure 6: Photograph of the mortar block immersed in water: (a) contrast sample and (b) hydrophobic sample and after abrasion with 240-grit sandpaper for (c) 0.3 mm, (d) 5.3 mm, and (e) 10.4 km. (f) Mass loss rate after polishing.

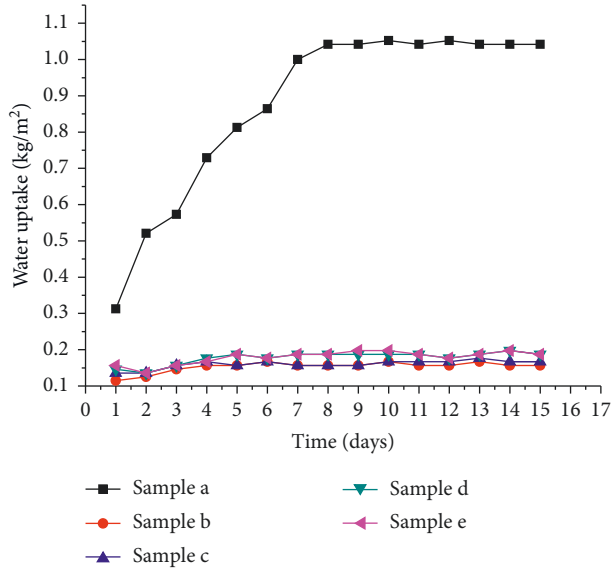

Figure 7: Effect of length reduction on water absorption of the hydrophobic sample.

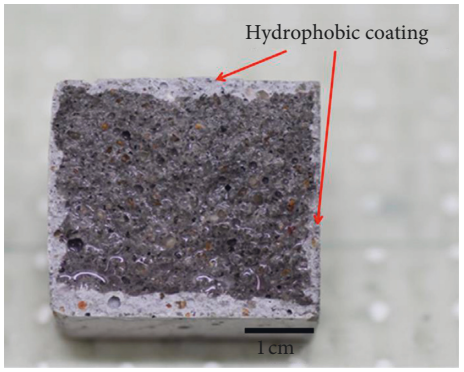

Figure 8: Photograph of the hydrophobic coating's thickness.

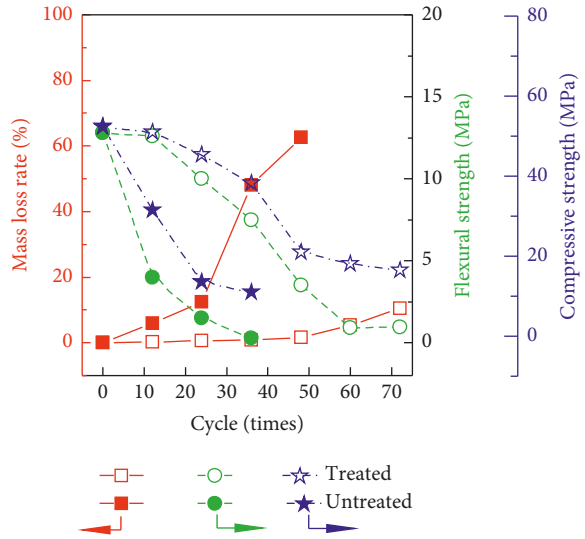

Figure 9: Mass loss rate (■ and □) and flexural (● and ○) and compressive (★ and ☆) strengths of the hydrophobic sample (□, ○, and ☆) and baseline sample (■, ●, and ★) measured after FTC tests.

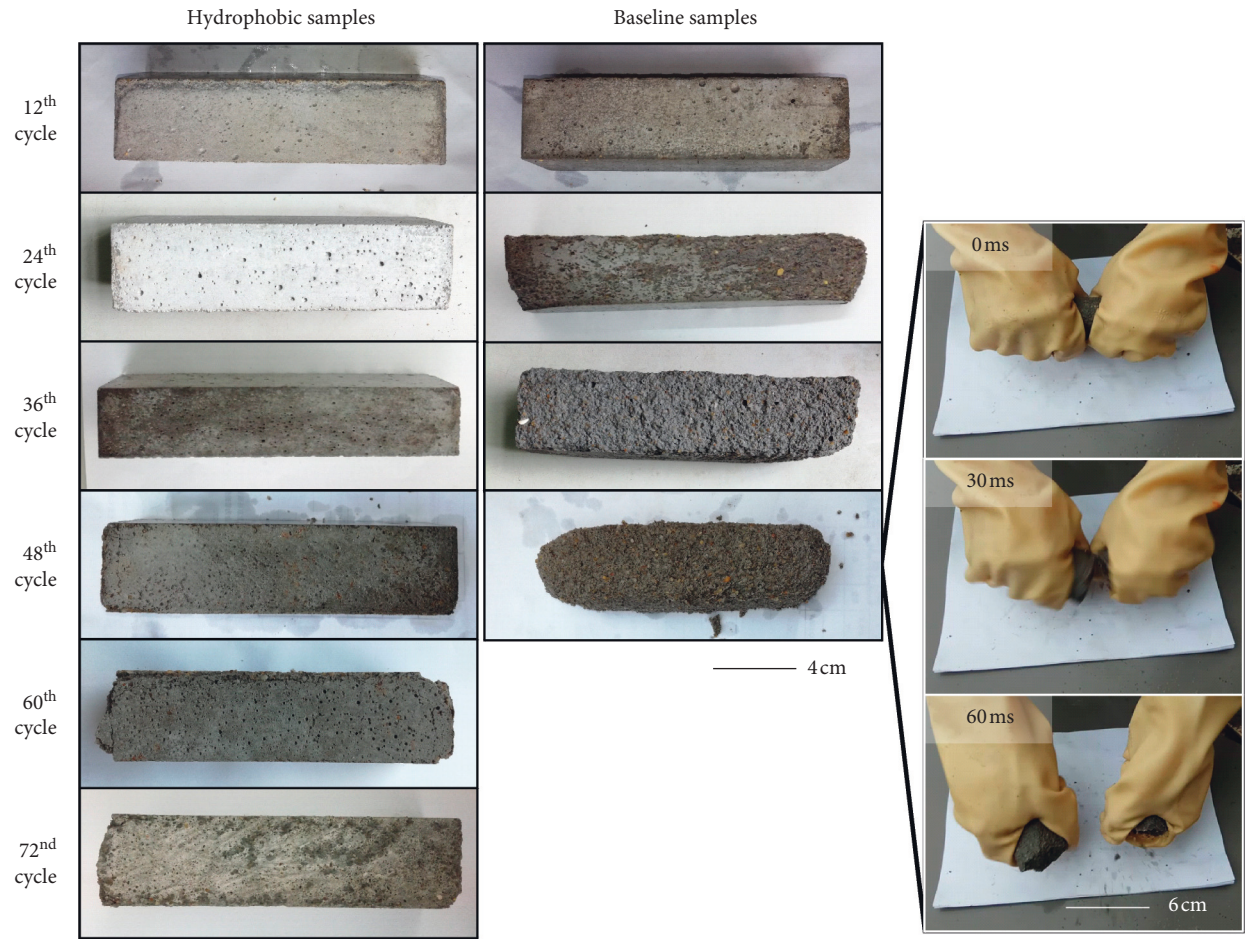

Figure 10: Photographs of the sample after different FTC tests.

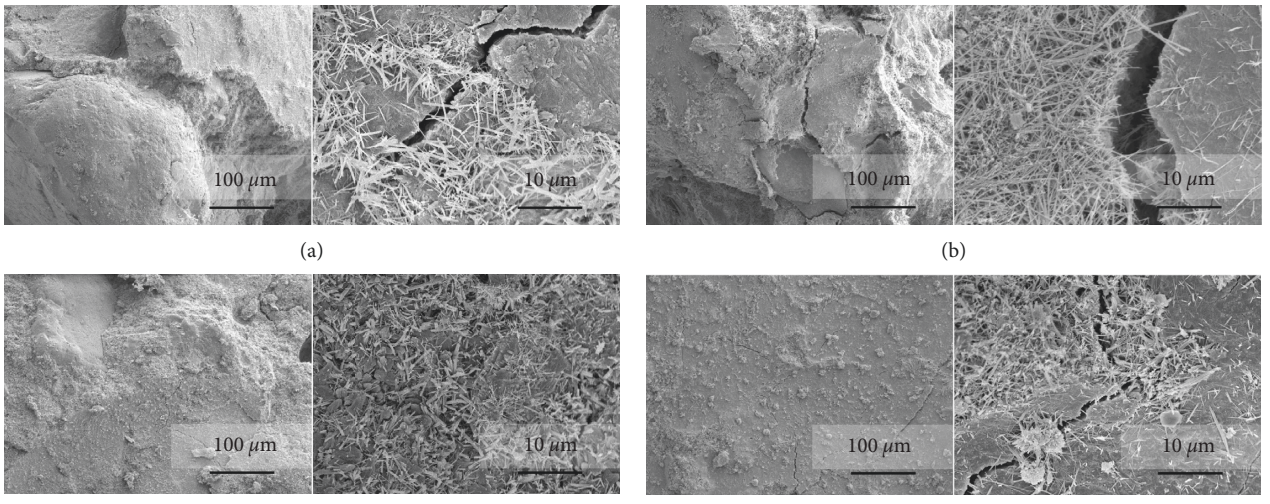

Figure 11: Continued.

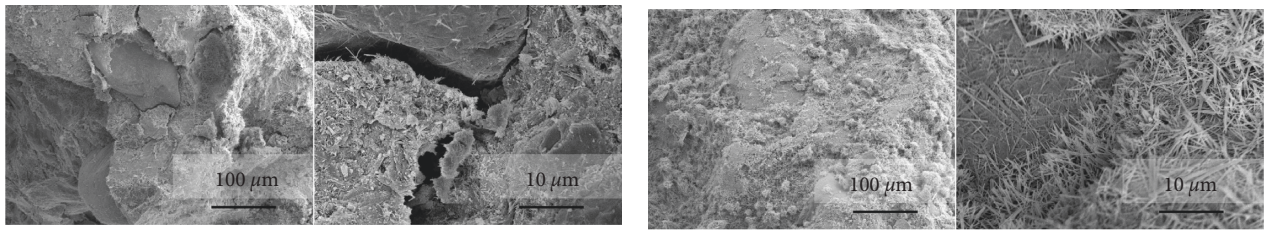

Figure 11: Micrographs of the mortar sample. Sectional microstructure of the baseline sample at the (a) 12th and (b) 36th FTCs. Sectional microstructure of the hydrophobic sample at the (c) 12th, (d) 36th, and (e) 72nd FTCs. (f) Microstructure of the hydrophobic coating on the hydrophobic sample at the 72nd FTC.

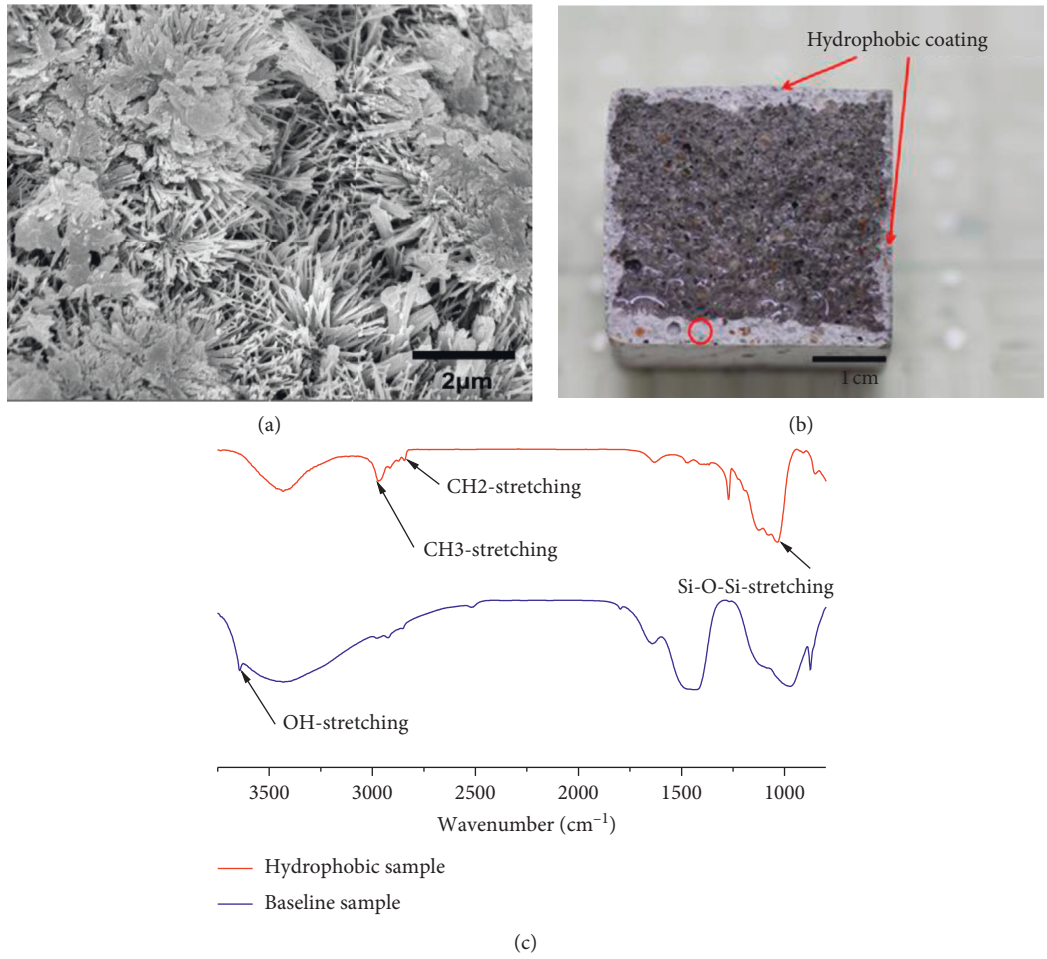

Figure 12: Microscopic analysis and chemical characterization of the hydrophobic coating: (a) hydrophobic sample, (b) SEM photograph of the hydrophobic coating, and (c) FT-IR spectra of the sample.

hydration products was characterized by the FT-IR. As shown in Figure 12(c), the FT-IR wavenumbers ranged from 3750 cm^{-1} to 1000 cm^{-1}. The absorption peak at 3644 cm^{-1} was attributed to the stretching vibration of -OH from Ca $(OH)_2$. The -OH stretching vibration peaks of $Ca(OH)_2$ were only observed in the baseline sample. This indicates that hydroxyl groups are consumed in the reaction of calcium hydroxide with iso-octyltriethoxysilane. Absorption peaks at 2970 cm^{-1} and 2920 cm^{-1} were observed in the hydrophobic coating, corresponding to $-CH_3$ and $-CH_2$ groups, respectively, implying that chemical bonds are formed between the coating and cement hydration products. The hydrophobic coating peak at 1130 cm^{-1} corresponds to the Si-O-Si group, which shows that continuous self-assembled molecular films are formed on the surface of hydration products.

4. Conclusions

This study aimed to transform a porous, hydrophilic cement mortar surface into a hydrophobic surface by chemical modification. Through hydrolysis and condensation, iso-octyltriethoxysilane forms continuous self-assembled molecular films on the surface of hydrated products, thus producing a hydrophobic coating with a thickness of 1–3 mm on the surface of the mortar. The WCA of the hydrophobic coating was 140°, and it had good waterproofing and wear resistance. A water absorption test showed that the cumulative water uptake of the hydrophobic samples decreased by 90%. Compared with a baseline sample, the mass loss rate and flexural and compressive strengths of the hydrophobic sample increased several-fold in the FTC test stages. Chemical bonding between iso-octyltriethoxysilane and cement hydration products ensures excellent wear resistance of the hydrophobic coating. In conclusion, the hydrophobic coating prepared by vacuum impregnation has an excellent protective effect on cement-based materials, and this technology has a wide range of applications in the building industry. Future work will focus on the preparation of hydrophobic coatings with higher thicknesses and better waterproofing performances via a simpler process.

Data Availability

All the data in this study are original.

Conflicts of Interest

The authors declare that they have no conflicts of interest.

Acknowledgments

This work was supported by the National Key R&D Plan (grant no. 2016YFC0701004), the Sichuan Science and Technology Program (no. 2019ZDZX0024), and the Doctoral Research Foundation of Southwest University of Science and Technology (18zx7134).

References

[1] N. R. Rakhimova, R. Z. Rakhimov, Y. N. Osin et al., "Solidification of nitrate solutions with alkali-activated slag and slag-metakaolin cements," *Journal of Nuclear Materials*, vol. 457, pp. 186–195, 2015.

[2] S. Chatterji, "Aspects of the freezing process in a porous material-water system," *Cement and Concrete Research*, vol. 29, no. 4, pp. 627–630, 1999.

[3] M. J. Setzer, "Mechanical stability criterion, triple-phase condition, and pressure differences of matter condensed in a porous matrix," *Journal of Colloid and Interface Science*, vol. 235, no. 1, pp. 170–182, 2001.

[4] L. Liu, S. Wu, H. Chen, and Z. Haitao, "Numerical investigation of the effects of freezing on micro-internal damage and macro-mechanical properties of cement pastes," *Cold Regions Science and Technology*, vol. 106-107, pp. 141–152, 2014.

[5] M. K. Ismail and A. A. A. Hassan, "Abrasion and impact resistance of concrete before and after exposure to freezing and thawing cycles," *Construction and Building Materials*, vol. 215, pp. 849–861, 2019.

[6] S. Pilehvar, A. M. Szczotok, J. F. Rodríguez et al., "Effect of freeze-thaw cycles on the mechanical behavior of geopolymer concrete and portland cement concrete containing micro-encapsulated phase change materials," *Construction and Building Materials*, vol. 200, pp. 94–103, 2019.

[7] H.-S. Shang and T.-H. Yi, "Freeze-thaw durability of air-entrained concrete," *Scientific World Journal*, vol. 2013, Article ID 650791, 6 pages, 2013.

[8] S. Jin, J. Zhang, and B. Huang, "Fractal analysis of effect of air void on freeze-thaw resistance of concrete," *Construction and Building Materials*, vol. 47, pp. 126–130, 2013.

[9] W. Micah Hale, S. F. Freyne, and B. W. Russell, "Examining the frost resistance of high performance concrete," *Construction and Building Materials*, vol. 23, no. 2, pp. 878–888, 2009.

[10] R. Zhao, Y. Yuan, Z. Cheng et al., "Freeze-thaw resistance of class F fly ash-based geopolymer concrete," *Construction and Building Materials*, vol. 222, pp. 474–483, 2019.

[11] F. U. A. Shaikh and S. W. M. Supit, "Compressive strength and durability properties of high volume fly ash (HVFA) concretes containing ultrafine fly ash (UFFA)," *Construction and Building Materials*, vol. 82, pp. 192–205, 2015.

[12] A. Salas, S. Delvasto, R. M. de Gutierrez, and D. Lange, "Comparison of two processes for treating rice husk ash for use in high performance concrete," *Cement and Concrete Research*, vol. 39, no. 9, pp. 773–778, 2009.

[13] J. Nam, G. Kim, B. Lee, R. Hasegawa, and Y. Hama, "Frost resistance of polyvinyl alcohol fiber and polypropylene fiber reinforced cementitious composites under freeze thaw cycling," *Composites Part B: Engineering*, vol. 90, pp. 241–250, 2016.

[14] S. N. Pogorelov and G. S. Semenyak, "Frost resistance of the steel fiber reinforced concrete containing active mineral additives," *Procedia Engineering*, vol. 150, pp. 1491–1495, 2016.

[15] I. Vegas, J. J. Gaitero, J. Urreta, R. García, and M. Frías, "Aging and durability of ternary cements containing fly ash and activated paper sludge," *Construction and Building Materials*, vol. 52, pp. 253–260, 2014.

[16] M. I. Khan and R. Siddique, "Utilization of silica fume in concrete: review of durability properties," *Resources, Conservation and Recycling*, vol. 57, pp. 30–35, 2011.

[17] B. B. Sabir, "Mechanical properties and frost resistance of silica fume concrete," *Cement and Concrete Composites*, vol. 19, no. 4, pp. 285–294, 1997.

[18] P. Zhang and Q.-f. Li, "Effect of silica fume on durability of concrete composites containing fly ash," *Science and Engineering of Composite Materials*, vol. 20, no. 1, pp. 57–65, 2013.

[19] H.-S. Kim, S.-H. Lee, and H.-Y. Moon, "Strength properties and durability aspects of high strength concrete using Korean metakaolin," *Construction and Building Materials*, vol. 21, no. 6, pp. 1229–1237, 2007.

[20] P. Duan, Z. Shui, W. Chen, and C. Shen, "Enhancing microstructure and durability of concrete from ground granulated blast furnace slag and metakaolin as cement replacement materials," *Journal of Materials Research and Technology*, vol. 2, no. 1, pp. 52–59, 2013.

[21] P. Reiterman, O. Holčapek, O. Zobal, and M. Keppert, "Freeze-thaw resistance of cement screed with various supplementary cementitious materials," *Reviews on Advanced Materials Science*, vol. 58, no. 1, pp. 66–74, 2019.

[22] F. B. P. D. Costa, D. P. Righi, A. G. Graeff, and L. C. P. d. Silva Filho, "Experimental study of some durability properties of

ECC with a more environmentally sustainable rice husk ash and high tenacity polypropylene fibers," *Construction and Building Materials*, vol. 213, pp. 505–513, 2019.

[23] C.-S. Shon, A. Abdigaliyev, S. Bagitova, C.-W. Chung, and D. Kim, "Determination of air-void system and modified frost resistance number for freeze-thaw resistance evaluation of ternary blended concrete made of ordinary portland cement/silica fume/class F fly ash," *Cold Regions Science and Technology*, vol. 155, pp. 127–136, 2018.

[24] A. S. Gill and R. Siddique, "Strength and micro-structural properties of self-compacting concrete containing metakaolin and rice husk ash," *Construction and Building Materials*, vol. 157, pp. 51–64, 2017.

[25] L. Feng, S. Li, Y. Li et al., "Super-hydrophobic surfaces: from natural to artificial," *Advanced Materials*, vol. 14, no. 24, pp. 1857–1860, 2002.

[26] D. Zang, R. Zhu, W. Zhang et al., "Corrosion-resistant superhydrophobic coatings on Mg alloy surfaces inspired by Lotus seedpod," *Advanced Functional Materials*, vol. 27, no. 8, pp. 1–7, 2017.

[27] X. Gao, X. Yan, X. Yao et al., "The dry-style antifogging properties of mosquito compound eyes and artificial analogues prepared by soft lithography," *Advanced Materials*, vol. 19, no. 17, pp. 2213–2217, 2007.

[28] X. Gao and L. Jiang, "Biophysics: water-repellent legs of water striders," *Nature*, vol. 432, no. 7013, p. 36, 2004.

[29] S. Mokhtari, F. Karimzadeh, M. H. Abbasi, and K. Raeissi, "Development of super-hydrophobic surface on Al 6061 by anodizing and the evaluation of its corrosion behavior," *Surface and Coatings Technology*, vol. 324, pp. 99–105, 2017.

[30] Y. Gao, L. Qu, B. He, K. Dai, Z. Fang, and R. Zhu, "Study on effectiveness of anti-icing and deicing performance of superhydrophobic asphalt concrete," *Construction and Building Materials*, vol. 191, pp. 270–280, 2018.

[31] C.-W. Lin, C.-J. Chung, C.-M. Chou, and J.-L. He, "Morphological effect governed by sandblasting and anodic surface reforming on the super-hydrophobicity of AISI 304 stainless steel," *Thin Solid Films*, vol. 620, pp. 88–93, 2016.

[32] E. M. Elnaggar, T. M. Elsokkary, M. A. Shohide, B. A. El-Sabbagh, and H. A. Abdel-Gawwad, "Surface protection of concrete by new protective coating," *Construction and Building Materials*, vol. 220, pp. 245–252, 2019.

[33] R. N. Wenzel, "Resistance of solid surfaces to wetting by water," *Industrial & Engineering Chemistry*, vol. 28, no. 8, pp. 988–994, 1936.

[34] W. She, X. Wang, C. Miao et al., "Biomimetic superhydrophobic surface of concrete: topographic and chemical modification assembly by direct spray," *Construction and Building Materials*, vol. 181, pp. 347–357, 2018.

[35] F. Tittarelli and G. Moriconi, "Comparison between surface and bulk hydrophobic treatment against corrosion of galvanized reinforcing steel in concrete," *Cement and Concrete Research*, vol. 41, no. 6, pp. 609–614, 2011.

[36] I. Flores-Vivian, V. Hejazi, M. I. Kozhukhova, M. Nosonovsky, and K. Sobolev, "Self-assembling particle-siloxane coatings for superhydrophobic concrete," *ACS Applied Materials & Interfaces*, vol. 5, no. 24, pp. 13284–13294, 2013.

[37] Z. Liu and W. Hansen, "Effect of hydrophobic surface treatment on freeze-thaw durability of concrete," *Cement and Concrete Composites*, vol. 69, pp. 49–60, 2016.

[38] Z. Song, X. Xue, Y. Li et al., "Experimental exploration of the waterproofing mechanism of inorganic sodium silicate-based concrete sealers," *Construction and Building Materials*, vol. 104, pp. 276–283, 2016.

[39] S. Weisheit, S. H. Unterberger, T. Bader, and R. Lackner, "Assessment of test methods for characterizing the hydrophobic nature of surface-treated high performance concrete," *Construction and Building Materials*, vol. 110, pp. 145–153, 2016.

[40] H. Herb, A. Gerdes, and G. Brenner-Weiß, "Characterization of silane-based hydrophobic admixtures in concrete using TOF-MS," *Cement and Concrete Research*, vol. 70, pp. 77–82, 2015.

[41] A. Arabzadeh, H. Ceylan, S. Kim et al., "Superhydrophobic coatings on portland cement concrete surfaces," *Construction and Building Materials*, vol. 141, pp. 393–401, 2017.

[42] H. Husni, M. R. Nazari, H. M. Yee et al., "Superhydrophobic rice husk ash coating on concrete," *Construction and Building Materials*, vol. 144, pp. 385–391, 2017.

[43] H. S. Wong, R. Barakat, A. Alhilali, M. Saleh, and C. R. Cheeseman, "Hydrophobic concrete using waste paper sludge ash," *Cement and Concrete Research*, vol. 70, pp. 9–20, 2015.

[44] M. Horgnies and J. J. Chen, "Superhydrophobic concrete surfaces with integrated microtexture," *Cement and Concrete Composites*, vol. 52, pp. 81–90, 2014.

[45] P. Scarfato, L. Di Maio, M. L. Fariello, P. Russo, and L. Incarnato, "Preparation and evaluation of polymer/clay nanocomposite surface treatments for concrete durability enhancement," *Cement and Concrete Composites*, vol. 34, no. 3, pp. 297–305, 2012.

[46] P. Reiterman, "Influence of metakaolin additive and nanoparticle surface treatment on the durability of white cement based concrete," *European Journal of Environmental and Civil Engineering*, pp. 1–14, 2018.